Apparent delay analysis for a flat-plate solar field model designed for control purposes

Gary Ampuño[1], Lidia Roca[2], Juan D. Gil[3], Manuel Berenguel[3] and Julio E. Normey-Rico[4]

[1] Universidad Politécnica Salesiana, Guayaquil (Ecuador)

[2] CIEMAT-Plataforma Solar de Almería, Centro Mixto CIESOL, Tabernas, (Spain)

[3] Universidad de Almería, Centro Mixto CIESOL, ceiA3, Almería, (Spain)

[4] Federal University of Santa Catarina, Department of Automation and Systems, Florianópolis, (Brazil)

Abstract

This study presents an analysis of the effect of the transport delay which occurs in solar flat-plate collector fields and how to include its behavior in dynamic models suitable for control purposes. This investigation has been carried out using simplified models based on dynamic energy balances and models based on step response methods and experimental tests. The solar flat-plate collector field encompasses parallel absorber pipes intertwined with pipelines which act as several first-order plus dead time systems in parallel. The effect is an apparent delay observed at the outlet temperature that must be included in the dynamic model in order to reduce the error between the real measurement and the model prediction. The main contribution of this paper is the procedure to evaluate the apparent delay to obtain adequate dynamic models aimed to be used for control purposes.

Keywords: *dynamic simulation, solar energy, bilinear model*

1. Introduction

The major purpose of a distributed solar collector (DSC) field is to collect the maximum solar energy available to produce as much thermal energy as possible. This thermal energy can be used for different processes such as electricity generation or seawater desalination (Camacho *et al.*, 1997; Ali *et al.*, 2011). An improvement of the process operation can be usually attained by controlling the outlet temperature of the solar field. In addition, the use of solar energy mitigates the impact of greenhouse emissions, especially the CO_2 caused by different kinds of industrial processes (Ackermann *et al.*, 2015).

Various types of solar thermal collectors and their applications are presented in (Camacho *et al.*, 2012), including flat-plate, compound parabolic, evacuated tube, parabolic-trough, Fresnel lens, parabolic dish and heliostat fields. As described in (Kalogirou, 2004; Duffie and Beckman, 2013), flat-plates are non-tracking collectors with a ‘‘black’’ solar energy-absorbing surface designed to transfer the absorbed energy to a fluid, a transparent cover reduces convection and radiation heat losses to the atmosphere and a back insulation reduces conduction heat losses. In order to evaluate and improve the system performance, mathematical modeling is an important and established widely used tool.

A detailed review of different models for flat-plate solar collectors can be found in (Nayak and Amer, 2000; Tagliafico *et al.*, 2014). Two of the most common models are the steady-state model following the ASHRAE 93-77 standard and the quasi-dynamic model described in the EN 12975 standard (Fischer *et al.*, 2004). Both models describe an energy balance but while the ASHRAE 93-77 model considers only the effect of the beam radiation and heat losses, the quasi-dynamic model adds the effect of the diffuse radiation, wind effects, and a heat losses term to describe the long-wave radiation. These models are mainly used for thermal performance characterization or for long-time evaluations. But, for transient studies, dynamic models are required (Kicsiny, 2017; Aleksiejuk *et al*., 2018).

Regarding dynamic models based on energy balance equations, classifications in literature are based on the number of differential equations considered. The one-node lumped parameter model consists on one differential equation for the fluid, it is easy to implement and the results obtained are quite satisfactory. One example can be found in (Pasamontes *et al.*, 2009) in which a flat-plate solar collector field is modeled to evaluate the water temperature that flows to an absorption heat pump or in (Gil *et al.*, 2018) in which a small flat-plate solar field provides thermal energy to a membrane distillation system. The two-node lumped parameter models add a differential equation to consider the temperature of the absorber plate and a heat transfer term to include the convection from the absorber plate to the heat transfer fluid. In (Deng *et al.*, 2015) these two equations are combined to eliminate the dependence with the absorber plate temperature and to reach a second-order differential equation for the heat transfer fluid. From a validation process described in (Deng *et al.*, 2017), authors emphasize the importance of reducing the temperature measurement error to make useful the second order term in the differential equation.

Distributed parameter models based on energy balance in the absorber plate and in the heat transfer fluid have also been used and validated with good results for the case of flat-plate solar collectors (Pasamontes *et al.*, 2013). In this case the energy balance is described by partial differential equations and the temperature can be evaluated along the absorber tube dividing the model in different control volumes. When high accuracy is required for the evaluation of the temperature or velocity inside tubes, computational fluid dynamic (CFD) software is a suitable tool. This kind of models include continuity, momentum and energy balances for the heat transfer fluids in three dimensions and they can be very useful for design optimization. In the study developed by (Facão, 2016) a CFD analysis is carried out with the aim of designing the manifolds in a flat-plate collector which improves the flow distribution along the absorber tubes.

Nevertheless, for control purposes, simplified dynamic models are required to make the control algorithms more efficient from the computational point of view. Although one-node lumped parameter models can be very useful as commented previously, transfer functions (Buzás and Kicsiny, 2014; Kicsiny, 2017; Aleksiejuk *et al.*, 2018), and black-box identification (Brus and Zambrano, 2010) are other techniques used to model flat-plate collectors. In the first case, authors obtain different transfer functions (one for each input) based on one-node lumped parameter model. In the second case, the model is obtained using a recursive prediction error method.

One issue that it is not completely tackled in flat-plate solar collector models is the delay. The most common delay included in the models is the one related directly with the transport delay in the inlet temperature such as in (Pasamontes *et al.*, 2009). This delay varies because of the transport time the heat transfer fluid takes to reach the sensor, it depends on the fluid flow rate and can be evaluated using the approximation proposed by (Normey-Rico *et al.*, 1998). (Brus and Zambrano, 2010) added two delays affecting the outlet temperature caused by two inputs; the flow rate and irradiance. From experimental data, linear approximations are obtained to evaluate these delays and to include them in the developed model. But, the source of these delays is not explained.

This paper focuses on a flat-plate solar field model putting emphasis on the delay treatment; the source of the delay, how to include the delay in a lumped parameter model and approximations to reduce the computational time to use the model for control purposes. This paper follows a previous paper (Ampuño *et al.*,2018) where the flat-plate collector dynamic model was presented. In that paper, the delays were experimentally obtained and included in the model. This new paper focuses in analyzing the causes of the observed delay, it demonstrates the existence of an apparent delay and the equations obtained are included in the model to improve the results, especially under transient conditions.

The paper is organized as follows: first, AQUASOL-II plant is shown in section 2, then the bilinear model, experimental campaign, calibration and validation results are shown in section 3, in section 4 the delay treatment and the models considered are explained, in section 5 a simplified model to reduce the computational time and make the model easier to be used for control purposes is proposed and in section 6 experimental results are fully discussed. Some concluding remarks are included at the end.

2. System description

The solar desalination facility AQUASOL-II (see Fig. 1) is placed at Plataforma Solar de Almeria (PSA), a dependency of the Centro de Investigaciones Energéticas, Medioambientales y Tecnológicas (CIEMAT) in the south of Spain, which is the largest concentrating solar technology research, development and test center in Europe. This facility has a flat-plate solar field which provides thermal energy to a Multi-Effect Desalination (MED) system (Fernández *et al.*, 2012; Alarcón *et al.*, 2005, 2007, 2010) and to a membrane distillation (MD) system, and was designed and built with the purpose of piloting studies of large-aperture static solar collector panels when joined with desalination processes. Fig. 1 displays the simplified schematic diagram of the plant. Basically, it is made of two main circuits: the primary circuit and the secondary circuit. Heat generation is performed in the primary circuit. Thermal storage to be used for the MED unit takes place at the secondary circuit.

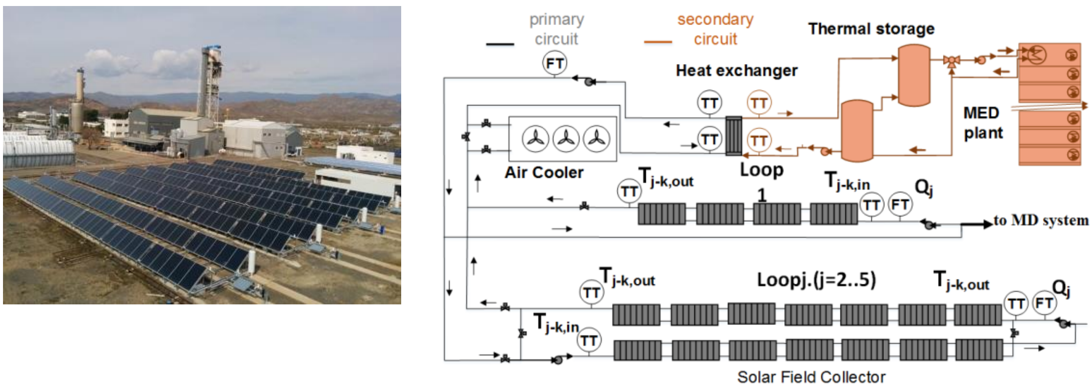

Fig. 1: Schematic diagram of the solar MED facility at PSA and photo of the solar field.

As shown in (Ampuño *et al*.,2018) the primary circuit is constituted by a solar field, an air cooler, and a heat exchanger and connection pipes. The static solar field has 60 collectors arranged in five loops linked in parallel. There are four loops with 14 flat-plate collectors each (each loop has two rows or sections connected in series with 7 collectors in parallel per row) and one loop with 4 flat-plate collectors connected in parallel. Each loop has its own pumping system so it can be operated independently. As the main energy source, the solar irradiance, cannot be controlled (it acts as a disturbance from the control viewpoint), the outlet temperature of the solar field is usually controlled by manipulating the fluid flow rate using the pumps (Roca *et al*., 2009).

Depending on the operating requirements (solar field characterization, desalination, process heat, …) the hot fluid from the solar field enters an air cooler or directly reaches a heat exchanger to heat the primary water circuit where thermal storage tanks are placed. Table 1 describes the nomenclature used in this work.

3. Bilinear model for a solar-field loop

A solar collector field can be described by a concentrated parameter model of the temperature. The model presented in (Roca *et al*., 2008, 2009) has been used as reference (see Eq. (1)). This concentrated parameters model, which provides the evolution of the temperature at the outlet of loop j section w, $T_{j,w,out}(t)$, has been applied to each section of each loop independently. The model considers that the behavior of each loop-section can be characterized taking into account just one flat-plate absorber tube and that the loop water flow rate is equally divided in each tube. Therefore, the volumetric flow rate considered as input in this model is Q_j/c_f where parameter c_f includes the number of tubes in each loop-section and the L·min^{-1}-L·s^{-1} conversion factor**.**

$$\rho c_p A_{cs} \frac{\partial T_{j,w,out}(t)}{\partial t} = \beta I(t) - \frac{H}{L}\big(T_m(t) - T_a(t)\big) - c_p \frac{\rho}{c_f} Q_j(t) \frac{\big(T_{j,w,out}(t) - T_{j,w,in}(t)\big)}{L}, \tag{1}$$

$$T_m(t) = \frac{T_{j,w,out}(t) + T_{j,w,in}(t)}{2}. \quad (2)$$

As explained in (Ampuño *et al.*, 2018), the outlet temperature of the loop depends on several inputs, the manipulated one, $Q_j(t)$ is the volumetric flow [L·min^{-1}], and the other ones act as disturbances: the inlet temperature, $T_{j,w,in}(t)$, the ambient temperature, $T_a(t)$, and the solar irradiance, $I(t)$. The remaining parameters are shown in Table 1.

Table 1: Nomenclature

Symbol	Quantity	Unit
A	Cross-section area of the loop pipe	m^2
A_{cs}	Collector absorber cross-section area	m^2
β	Parameter that modulates the solar irradiance	m
c_p	Specific heat capacity	J·kg^{-1}·ºC^{-1}
c_f	Conversion factor to account for number of flat-plate tubes in each loop, and L·min^{-1} – L·s^{-1} conversion	s·L·min^{-1}·m^{-3}
c_{f2}	Conversion factor to account for L·min^{-1} – m^3·s^{-1} conversion	s·L·min^{-1}·m^{-3}
$d_{j,w,l,in}$	Transport delay in the incoming water to each one of the absorber pipes that are connected in parallel of DSC loop j ($j = 1..5$) section w (w =1..2) absorber pipes number *l (l =1..350)*	s
$d_{j,w,l,out}$	Transport delay in the outlet water from each one of the absorber pipes that are connected in parallel of DSC loop j ($j = 1..5$) section w (w =1..2) absorber pipes number *l (l =1..350)*	s
$d_{j,tout-tin}$	Inlet - outlet water temperature related transport delay in loop j ($j = 1..5$)	s
$d_{j,tout-Q}$	Inlet water flow rate - outlet water temperature related apparent delay in loop j ($j = 1..5$)	s
$d_{j,tout-I}$	Inlet solar irradiance - outlet water temperature related apparent delay in loop j ($j = 1..5$)	s
$d_{j,tout-tin,s}$	Inlet-outlet water temperature related transport delay in loop j ($j = 1..5$) for the simplified model	s
$d_{j,tout-Q,s}$	Inlet water flow rate - outlet water temperature related apparent delay in loop j ($j = 1..5$) for the simplified model	s
$d_{j,tout-I,s}$	Inlet solar irradiance-outlet water temperature related apparent delay in loop j ($j = 1..5$) for the simplified model	s
H	Thermal losses coefficient	J·s^{-1}· ºC^{-1}
I	Solar irradiance	W·m^{-2}
L	Absorber pipe length	m
L_{ca}	Distance between two absorber pipes	m
L_{loop}	Length of the flat-plate collector loop	m
n	Number of absorber pipes in each loop-section (n=200 for DSC loop 1 and n=350 for DSC loops j=2..5)	-
N	Number of samples	-
Q_j	Volumetric flow of DSC loop j ($j = 1..5$)	L·min^{-1}
$Q_{ca,j,w,l}$	Water flow rate that circulates between absorber pipes l and l+1 *(l =1..n)* of DSC loop j ($j = 1..5$) section w (w =1..2)	L·min^{-1}
T_a	Ambient temperature	ºC
$T_{j,w,in}$	Inlet temperature of DSC loop j ($j = 1..5$) section w (w =1..2)	ºC
$T_{j,w,l,in}$	Inlet temperature of absorber pipe *l (l =1..n)*, DSC loop j ($j = 1..5$), section w (w =1..2)	ºC
$T_{j,w,out}$	Outlet temperature of DSC loop j ($j = 1..5$) section w (w =1..2)	ºC
$T_{j,w,l,out}$	Outlet temperature of absorber pipe *l (l =1..n)*, DSC loop j ($j = 1..5$) section w (w =1..2)	ºC

$T_{s,j,w,in}$	Inlet temperature measured by the sensor of DSC loop j ($j = 1..5$), section w (w =1..2)	ºC
$T_{s,j,w,out}$	Outlet temperature measured by the sensor of DSC loop j ($j = 1..5$), section w (w =1..2)	ºC
S_t	Sampling time	s
T_m	Equivalent flat plate tube mean temperature	ºC
v	Velocity rate	$m \cdot s^{-1}$
ρ	Water density	$kg \cdot m^{-3}$
y_i	Plant outputs at sample *i*	
$\hat{y}_i$	Model outputs at sample *i*	

3.1 Experimental campaign.

In order to calibrate and validate the solar field model, dynamic data from AQUASOL II facility was collected. The experimental campaign started on November 16th, 2016 and ended on December 21st, 2016. The following data details the methodology carried on to perform the tests:

- The secondary circuit of the AQUASOL II facility (see Fig. 1) is stopped, therefore no water flows between the heat exchanger and the thermal storage system.
- The solar field inlet temperature is maintained at different values using the air cooler. A PID controller with anti-windup regulates the air-cooler fan speed to maintain the desired temperature at the outlet of the air-cooler. Since the secondary circuit is stopped, the air-cooler outlet temperature can be considered as the solar field inlet temperature at steady-state conditions. The inlet temperature range considered is from 50 °C to 85 °C.
- Water flow rates in loops 3 to 5 have been varied between 18 $L \cdot min^{-1}$ and 36 $L \cdot min^{-1}$. Water flow rate in loop 1 has been varied between 7 $L \cdot min^{-1}$ and 18 $L \cdot min^{-1}$.
- Loop 2 was out of service during the experimental campaign.
- Tests were performed during sunny and cloudy days to analyze the effect of real irradiance disturbances in the model.
- The testing schedule ranges from 9:00am until 14:00pm local time.
- Three different kind of tests have been performed: a) solar field temperature remains constant during the whole test and flow rate changes are performed in each loop, b) flow rates remain constant during the whole test and inlet temperature changes are performed and c) inlet temperature and flow rate changes are performed at the same time.

3.2 Calibration.

Parameter calibration is usually a challenging task and its complexity rises with the number of unknown variables. In this work, two parameters must be calibrated; the irradiance parameter, β, and the thermal losses coefficient, H (see Eq. (1)). With the obtained information from the experimental campaign and the least squares method, these parameters were precisely and accurately calibrated. The least squares method is an optimization technique applied to linear in parameters systems. The aim is to find the model output, the outlet temperature in this case, that best approximates the real process output according to the minimal sum of squared error function, so that, the best combination of unknown parameters are obtained from this optimization. An outline of numerous least square concepts can be found in (Goodwin and Payne, 1977).

Following this method, the obtained unknown parameters are those shown in Table 2, where errors are depicted in terms of maximum error, ME, and the root mean square error, RMSE, estimated as:

$$RMSE = \sqrt{\frac{1}{N}\sum_{i=1}^{N}(y_i - \hat{y}_i)^2}\ , \tag{3}$$

N being the number of samples from the experiment, and y_i and $\hat{y}_i$ are the plant and model outputs at sample i. It is important to mention that the sampling time considered, S_t, is 1 s.

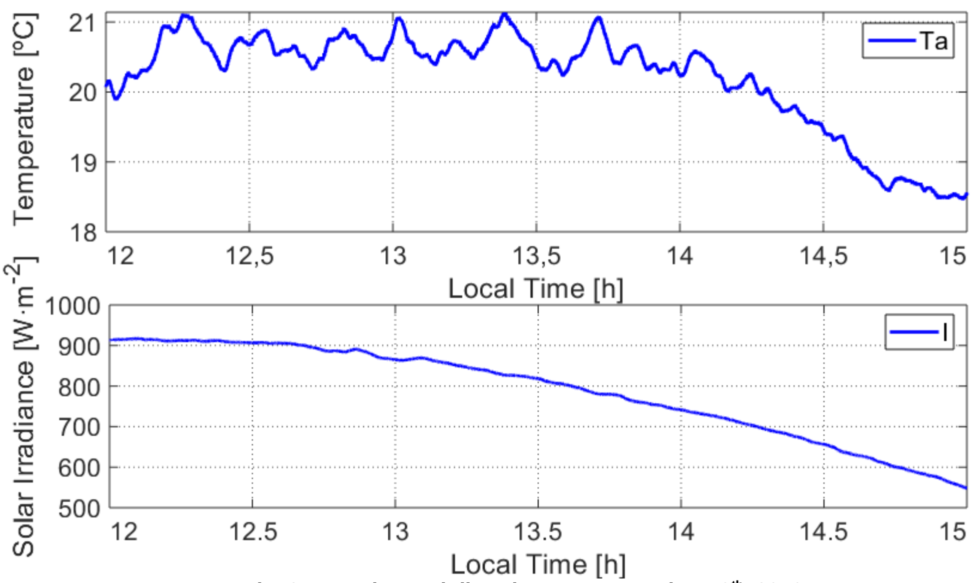

Fig. 2: Experimental disturbances, November 10th, 2016.

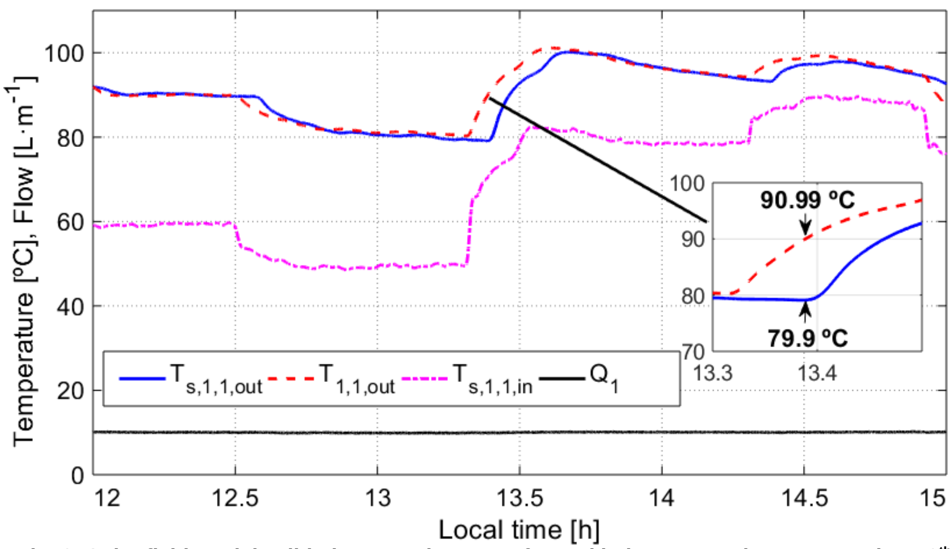

Fig. 3: Solar field model validation experiment performed in loop 1, section 1, November 10th, 2016.

The mean RMSE errors for each loop-section model are acceptable, but the ME error is far from the desired results. This huge deviation has been analyzed and it is caused by the delay between the outlet temperature and the different inputs (inlet temperature, water flow rate and irradiance). As shown in Fig. 3, if the model does not take into account the delay, huge errors can be obtained between the model response and the real data during transients. Notice for example the change performed at the inlet temperature of loop 1 section 1 between 13h and 13.5h; the real outlet temperature delays about 270 seconds to start increasing, which causes a maximum error of 11.1 °C. Section 4 goes into detail about the origin of this delay and how to model it.

3.3 Validation.

For the validation procedure, the performance of the model has been evaluated using a different data set. These tests present variability in all the inputs: irradiance, inlet temperature, ambient temperature and water flow rate.

One of the objectives of this study is to compare the solar field model under different kind of disturbances, such as variable solar irradiance due to passing clouds. On December 14th (shown in Fig. 4), cloudy conditions can be appreciated from local time 11:45am (11.75) until 12:30pm (125). For the case of loop 5 section 2 shown in Fig. 4, the water flow rate was maintained constant at 36 L·min^{-1} and the inlet temperature varies between 55 ºC and 75 ºC. This figure shows that the outlet temperature calculated by the model is similar to the real outlet temperature of the solar field in a clear day (from 10:30am to 11:45am). When hard disturbances in irradiance occur, the model behavior also shows sudden changes, conversely to the real data, that presents a smoother profile. Section 4 deals with this sudden solar radiation change.

This example also shows the delay effect between the two inputs, irradiance and inlet temperature, and the outlet temperature; when the clouds appear and the solar irradiance falls, the outlet temperature has a delay of around 216 seconds. Since the model does not include this delay, an error of 7.85 ºC is obtained.

Table 2: Validation campaign results using the bilinear model.

LOOP,SECTION	*PARAMETERS*		*GLOBAL ERROR*	
	H [J s^{-1} ºC^{-1}]	*β* [m]	*RMSE* [°C]	*ME* [°C]
5,1	*1.095*	*0.0959*	*2.410*	*11.790*
5,2	*1.106*	*0.0956*	*1.680*	*11.400*
4,1	*1.137*	*0.0949*	*1.640*	*7.900*
4,2	*1.159*	*0.097*	*1.560*	*10.810*
3,1	*1.101*	*0.0951*	*1.830*	*7.650*
3,2	*1.121*	*0.0946*	*1.690*	*10.890*
1	*1.107*	*0.094*	*1.790*	*7.550*

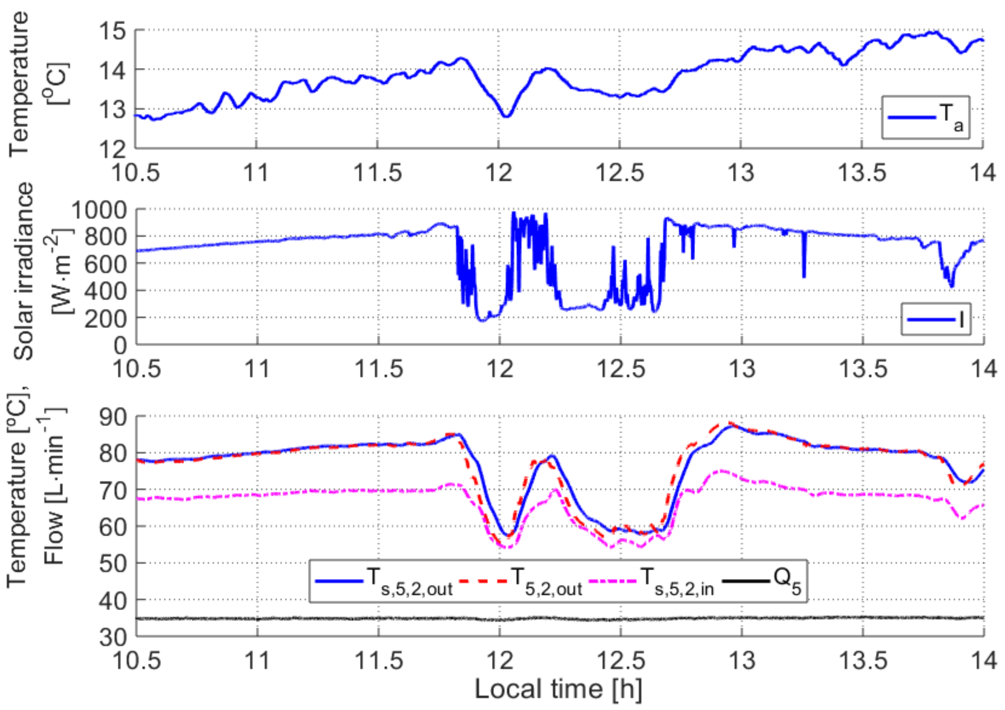

Fig. 4: Experimental disturbances and simulation results using the solar field model, loop 5, section 2, December 14th, 2016

Table 2 shows the RMSE and ME errors obtained in the validation campaign using the bilinear model for each solar-field loop section. Comparing the model results with real data, the ME errors are far from the expected results due to the fact that the delays observed in the real systems are not implemented in the model.

4. The apparent and transport delays.

Fig. 3 and 4 present a comparison between the temperature calculated by the model and the temperature measured at the end of the return pipe. These figures intend to demonstrate that the dynamics of the water temperature measured can be approximated using the proposed model described in Eq. (1) but it is mandatory to take into consideration a variable dead-time to avoid huge errors during transients. As will be explained in this section, the source of this delay that cause fluctuations in the behavior of the collector water outlet temperature is a transport delay at the inlet and outlet of each absorber pipe that produces an apparent delay at the outlet of the loop.

4.1 The transport delay.

Fig. 5 comprises three images showing the flat-plate collector solar field and how the absorber tubes are connected to each other. Since the inlet temperature sensor is located at the beginning of the loop ($T_{s,j,w,in}$), there is a transport delay in the incoming water to each one of the absorber pipes that are connected in parallel ($d_{j,w,l,in}$) where *j* is the loop number ($j \in [1,5]$), *w* the loop section ($w \in [1,2]$) and *l* the absorber tube number ($l \in [1,350]\ \forall\, j = \{2 \ldots 5\}, l \in [1,200]\ \forall\, j = 1$). This transport delay can be estimated at each sampling time as a flow-dependent delay as described by (Normey-Rico *et al.*, 1998).

$$T_{j,w,l,in}(t) \approx T_{s,j,w,in}\left(t - d_{j,w,l,in}\right), \tag{4}$$

$$L_{ca} = \int_{0}^{d_{j,w,l,in}} v(t)\, dt \rightarrow \frac{S_t}{A} \sum_{i=0}^{i=m-1} Q_{ca,j,w,l}(k-i) \cdot c_{f2} = L_{ca}, \tag{5}$$

where *k* is the actual sampling time, S_t [s] is the sampling time, $v(t)$ is the water velocity rate [m·s^{-1}], index m is equal to the delay (in sampling times), $Q_{ca,j,w,l}(k-i)$ [L·min^{-1}] is the flow rate at sampling time $k - i$ that circulates between two absorber tubes connections, cf2 is a conversion factor to account of the L·min^{-1} - m^3·s^{-1} conversion, *A* is the cross-section area of the loop pipe [m^2]; and the integral of $v(t)$ is approximated by a discrete time sum that accounts for different flow rates. The input, $T_{j,w,l,in}(t)$, is estimated in every sample time using past measures of the inlet temperature $T_{s,j,w,in}(t)$, and evaluating the delay $d_{j,w,l,in}$ with the past flow rates.

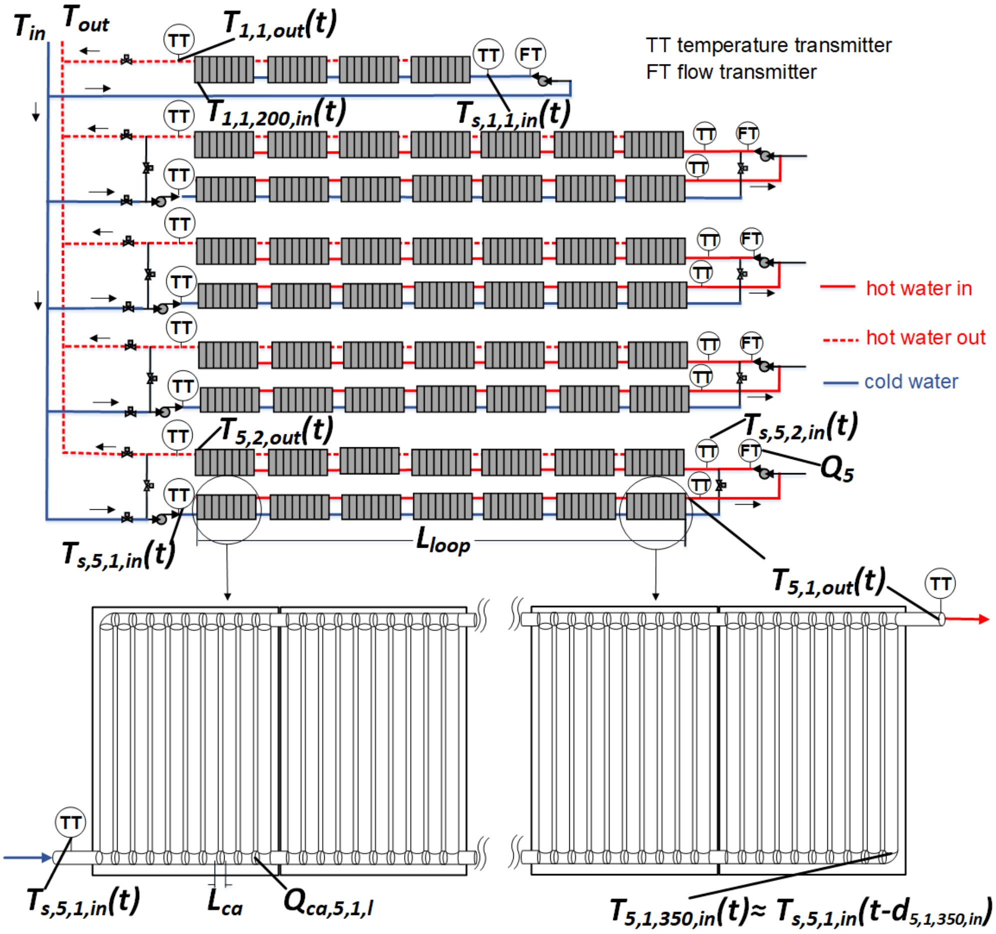

Fig. 5: AQUASOL II solar field and absorber tubes connections.

The procedure described in Eq. (5) must be repeated to estimate the inlet temperature for each absorber pipe inside the loop because the volumetric flow rate is different for each connection. With the aim of reducing the computational cost, it is possible to estimate the delay between the sensor located at the beginning of the loop and the inlet of each absorber pipe by only evaluating the delay between the sensor and the inlet of the last absorber pipe.

Since the distance between two absorber pipes is the same ($L_{ca=}L_{loop}/n$) and the volumetric flow rate inside each absorber pipe is the same (Q_j/n), it is easy to follow that the volumetric flow rate in the connection between absorber pipe l and $l+1$ can be estimated as:

$$Q_{ca,j,w,l,in} = Q_j\left(1-\frac{l}{n}\right) \qquad \forall\, l\ \in [1, n-1]. \tag{6}$$

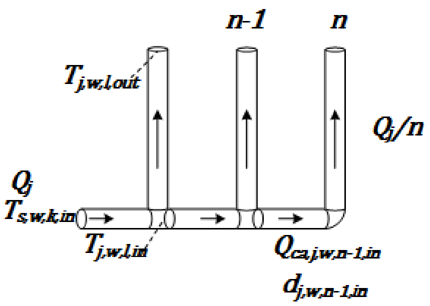

Fig. 6: Inlet temperature delay within the inlet distributer pipe.

Then, to estimate the delay $d_{j,w,(n-1),in}$ between absorber pipe $n-1$ and n, we have to consider the volumetric flow rate Q_j/n and the length L_{loop}/n in Eq. (5).

To calculate the delay between absorber pipe $n-2$ and $n-1$ with Eq. (5), it is necessary to consider the volumetric flow rate $2 \cdot Q_j/n$ and the length L_{loop}/n, but it is easy to deduce that this delay will exactly be the half of the one calculated previously because it is the time required to go across a pipe with the same cross section area and length but with the double volumetric flow rate. So, it can be concluded that:

$$d_{j,w,l,in} = \frac{d_{j,w,n-1}}{n-l} \qquad \forall\, l \in [1, n-1], \tag{7}$$

Notice that these delays are between the connections of two absorber pipes. The inlet temperature to each absorber pipe will be:

$$T_{j,w,l,in} = T_{s,j,w,in}\left(t - \sum_{i=1}^{i=l} d_{j,w,i}\right), \tag{8}$$

The other transport delay observed in the flat plate collectors is present at the outlet of the distributer pipe which affects to the loop outlet temperature $T_{j,w,out}$. Due to the connections between the absorber pipes in the upper part, the volumetric flow rate is different in each connection, giving rise to different transport delays. Using Eq. (5), it is possible to calculate the delay in each connection and to assess the delay between the outlet of each absorber tube and the sensor located at the outlet of the collector loop.

For this, the volumetric flow rate in the connection between absorber pipe l and $l+1$ can be estimated as:

$$Q_{ca,j,w,l,out} = \frac{l \cdot Q_j}{n} \qquad \forall\, l \in [1, n-1], \tag{9}$$

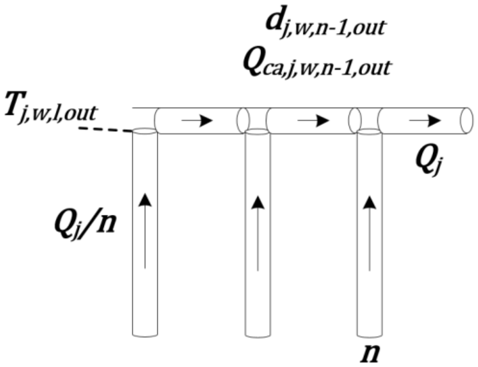

Fig. 7: Outlet temperature delay within the outlet distributer pipe.

Then, to estimate the delay $d_{j,w,1,out}$ between the absorber pipe 1 and 2 the volumetric flow rate Q_j/n and the length L_{loop}/n has to be considered in Eq. (5).

To calculate the delay between absorber tube *2* and *3* with Eq. (5), the volumetric flow rate $2 \cdot Q_j/n$ and the length L_{loop}/n have to be considered, but the number of equations can be simplified again following the same reasoning used previously:

$$d_{j,w,l,out} = \frac{d_{j,w,1}}{nl} \qquad \forall\, l \in [1, n]. \tag{10}$$

Notice that these delays are between the connections of two absorber tubes. The outlet temperature of the loop *j* section *w* will be:

$$T_{j,w,out}(t) = \frac{\sum_{i=1}^{i=n} T_{j,w,i,out}\left(t - \sum_{ii=1}^{ii=n} d_{j,w,ii}\right)}{n} \tag{11}$$

Therefore, to evaluate the water temperature at the outlet of each loop section, the temperature at the outlet of each absorber pipe has to be estimated, which requires solving 3000 bilinear equations described by Eq. (1). In order to reduce the required computational time, the concept of apparent delay is introduced in the following section to explain the approximation considered to evaluate the water temperature at the outlet of each loop-section.

4.2 The apparent delay.

As described by (Normey-Rico *et al*., 2007), when there are several systems connected in parallel, as happens in the absorber pipes, and each of them has a small delay, the accumulation of every one of these delays produces an apparent delay. In this case the apparent delay depends on the number of absorber pipes of the loop, n.

The idea behind this section is to evaluate the apparent delay observed when step changes are performed at the following inputs: flow rate, inlet temperature and irradiance. From these steps, first-order models are obtained, the results are compared with real data and expressions are obtained to evaluate those apparent delays as a function of the flow rate.

The linear approximation is usually found by the Taylor's series expansions of the non-linear vector field in the vicinity of a steady state (equilibrium). The approximation depends on the system parameters and the specific steady state (an explanation of nonlinear models linearization can be found in (Ogata, 1998)).

As a first stage, considering the first section of a collector loop, first-order models relating the water outlet temperature to each one of the inputs have to be obtained. These first-order models can be obtained from the bilinear model described in Eq. (1) for a steady state $\left(\rho c_p A_{cs} \frac{\partial T_{j,w,out}(t)}{\partial t} = 0\right)$.

$$0 = \beta \bar{I} - \frac{c_p \rho}{c_f L} \bar{Q}_j\left(\bar{T}_{j,w,out} - \bar{T}_{j,w,in}\right) - \frac{H}{L}\left(\frac{\bar{T}_{j,w,out} + \bar{T}_{j,w,in}}{2} - \bar{T}_a\right), \tag{12}$$

where the linearization is carried out around the operating points defined by $(\bar{Q}_j, \bar{T}_{j,w,out}, \bar{T}_{j,w,in}, \bar{T}_a, \bar{I})$. System variables $Q_j(t), T_{j,w,out}(t), T_{j,w,in}(t), T_a(t)$ and $I(t)$ are represented as the sum of the steady-state value that defines the operating point with the value of the deviation variable around that equilibrium state $(\tilde{Q}_j(t), \tilde{T}_{j,w,out}(t), \tilde{T}_{j,w,in}(t), \tilde{T}_a(t), \tilde{I}(t))$:

$$\begin{aligned} Q_j(t) &= \bar{Q}_j + \tilde{Q}_j(t), \\ T_{j,w,out}(t) &= \bar{T}_{j,w,out} + \tilde{T}_{j,w,out}(t), \\ T_{j,w,in}(t) &= \bar{T}_{j,w,in} + \tilde{T}_{j,w,in}(t), \\ T_a(t) &= \bar{T}_a + \tilde{T}_a(t), \\ I(t) &= \bar{I} + \tilde{I}(t), \end{aligned} \tag{13}$$

The deviation variables represent the linear dynamic system when variations occur in the dynamics of the system around the operating point defined by $(\bar{Q}_j, \bar{T}_{j,w,out}, \bar{T}_{j,w,in}, \bar{T}_a, \bar{I})$.

Using the Taylor's series approximation in the non-linear part of the model, the following linearization is obtained:

$$Q_j(t)T_{j,w,out}(t) \approx \bar{Q}_j\bar{T}_{j,w,out} + \frac{\partial Q_j(t)T_{j,w,out}(t)}{\partial Q_j(t)}\bigg|_{\bar{Q}_j,\bar{T}_{j,w,out}} \overbrace{\left(Q_j(t)-\bar{Q}_j\right)}^{\tilde{Q}_j(t)} +$$

$$\frac{\partial Q_j(t)T_{j,w,out}(t)}{\partial T_{j,w,out}(t)}\bigg|_{\bar{Q}_j,\bar{T}_{j,w,out}} \overbrace{\left(T_{j,w,out}(t)-\bar{T}_{j,w,out}\right)}^{\tilde{T}_{j,w,out}(t)},$$

$$Q_j(t)T_{j,w,in}(t) \approx \bar{Q}_j\bar{T}_{j,w,in} + \frac{\partial Q_j(t)T_{j,w,in}(t)}{\partial Q_j(t)}\bigg|_{\bar{Q}_j,\bar{T}_{j,w,in}} \overbrace{\left(Q_j(t)-\bar{Q}_j\right)}^{\tilde{Q}_j(t)} +$$

$$\frac{\partial Q_j(t)T_{j,w,in}(t)}{\partial T_{j,w,in}(t)}\bigg|_{\bar{Q}_j,\bar{T}_{j,w,in}} \overbrace{\left(T_{j,w,in}(t)-\bar{T}_{j,w,in}\right)}^{\tilde{T}_{j,w,in}(t)},$$

$$Q_j(t)T_{j,w,out}(t) \approx \bar{Q}_j\bar{T}_{j,w,out} + \bar{T}_{j,w,out}\tilde{Q}_j(t) + \bar{Q}_j\,\tilde{T}_{j,w,out}(t), \tag{14}$$

$$Q_j(t)T_{j,w,in}(t) \approx \bar{Q}_j\bar{T}_{j,w,in} + \bar{T}_{j,w,in}\tilde{Q}_j(t) + \bar{Q}_j\,\tilde{T}_{j,w,in}(t).$$

Since $\rho c_p A_{cs}\frac{\partial T_{j,w,out}(t)}{\partial t} = \rho c_p A_{cs}\frac{\partial \tilde{T}_{j,w,out}(t)}{\partial t}$, the bilinear model can be approximated as:

$$\begin{aligned}\rho c_p A_{cs}\frac{\partial \tilde{T}_{j,w,out}(t)}{\partial t} &= \beta\left(\bar{I}+\tilde{I}(t)\right) \\ &- \frac{c_p\rho}{c_f L}\Big(\left(\bar{Q}_j\bar{T}_{j,w,out} + \bar{T}_{j,w,out}\tilde{Q}_j(t) + \bar{Q}_j\,\tilde{T}_{j,w,out}(t)\right) \\ &- \left(\bar{Q}_j\bar{T}_{j,w,in} + \bar{T}_{j,w,in}\tilde{Q}_j(t) + \bar{Q}_j\,\tilde{T}_{j,w,in}(t)\right)\Big) \\ &- \frac{H}{L}\left(\frac{\bar{T}_{j,w,out} + \tilde{T}_{j,w,out}(t) + \bar{T}_{j,w,,in} + \tilde{T}_{j,w,in}(t)}{2} - \left(\bar{T}_a + \tilde{T}_a(t)\right)\right).\end{aligned}$$

Taking into account steady state relationships:

$$\begin{aligned}\rho c_p A_{cs}\frac{\partial \tilde{T}_{j,w,out}(t)}{\partial t} &= \overbrace{\beta\bar{I} - \frac{c_p\rho}{c_f L}\bar{Q}_j\bar{T}_{j,w,out} + \frac{c_p\rho}{c_f L}\bar{Q}_j\bar{T}_{j,w,in} - \frac{H}{L}\left(\frac{\bar{T}_{j,w,out}+\bar{T}_{j,w,in}}{2} - \bar{T}_a\right)}^{0} + \beta\tilde{I}(t) \\ &- \frac{c_p\rho}{c_f L}\bar{T}_{j,w,out}\tilde{Q}_j(t) - \frac{c_p\rho}{c_f L}\bar{Q}_j\,\tilde{T}_{j,w,out}(t) + \frac{c_p\rho}{c_f L}\bar{T}_{j,w,in}\tilde{Q}_j(t) + \frac{c_p\rho}{c_f L}\bar{Q}_j\,\tilde{T}_{j,w,in}(t) \\ &- \frac{H}{L}\left(\frac{\tilde{T}_{j,w,out}(t)+\tilde{T}_{j,w,in}(t)}{2} - \tilde{T}_a(t)\right),\end{aligned}$$

$$\begin{aligned}\rho c_p A_{cs}\frac{\partial \tilde{T}_{j,w,out}(t)}{\partial t} &= \beta\tilde{I}(t) - \frac{c_p\rho}{c_f L}\left(\left(\bar{T}_{j,w,out}-\bar{T}_{j,w,in}\right)\tilde{Q}_j(t) + \bar{Q}_j\,\left(\tilde{T}_{j,w,out}(t)-\tilde{T}_{j,w,in}(t)\right)\right) \\ &- \frac{H}{L}\left(\frac{\tilde{T}_{j,w,out}(t)+\tilde{T}_{j,w,in}(t)}{2} - \tilde{T}_a(t)\right).\end{aligned} \tag{15}$$

Considering that small variations of $\tilde{Q}_j(t)$, $\tilde{T}_{j,w,in}(t)$, $\tilde{T}_a(t)$ and $\tilde{I}(t)$ are produced around the equilibrium point $\tilde{Q}_j(\mathrm{t}) = \Delta Q_j$, $\tilde{T}_{j,w,in}(\mathrm{t}) = \Delta T_{j,w,in}$, $\tilde{T}_a(\mathrm{t}) = \Delta T_a$, $\tilde{I}(\mathrm{t}) = \Delta I$, a temporal evolution of $\tilde{T}_{j,w,out}(t)$ from $\bar{T}_{j,w,out}$ to a new state value $\bar{T}_{j,w,out} + \Delta T_{j,w,out}$ is produced and the linearized system can be represented by a first order model $\left(\tau\frac{\partial y(t)}{\partial t} + y(t) = ku(t)\right)$:

$$\underbrace{\frac{\rho c_p A_{cs}}{\left[\frac{c_p\rho\bar{Q}_j}{c_f L} + \frac{H}{2L}\right]}}_{\tau}\frac{\partial\tilde{T}_{j,w,out}(t)}{\partial t} + \tilde{T}_{j,w,out}(t) = \underbrace{\left[\frac{-\frac{c_p\rho}{c_f L}\left(\bar{T}_{j,w,out} - \bar{T}_{j,w,in}\right)}{\left[\frac{c_p\rho\bar{Q}_j}{c_f L} + \frac{H}{2L}\right]}\right]}_{k_Q}\tilde{Q}_j(t) + \underbrace{\frac{\beta}{\left[\frac{c_p\rho\bar{Q}_j}{c_f L} + \frac{H}{2L}\right]}}_{k_I}\tilde{I}(t) - \underbrace{1}_{k_{Tin}} \cdot \tilde{T}_{j,w,in}(t) + \underbrace{\frac{\frac{H}{L}}{\left[\frac{c_p\rho\bar{Q}_j}{c_f L} + \frac{H}{2L}\right]}}_{k_{Ta}}\tilde{T}_a(t). \quad (16)$$

For each absorber pipe and for each input, the steady-state gain and the time constant are almost the same (the properties of the water can be slightly different) but the output delay will be different according to the transport delay explained in section 4.1. Considering the first order models obtained for each absorber pipe, the outlet temperature of one loop section as a function of each one of the inputs u $(Q_j, I, T_{j,w,in}, T_a)$ can be evaluated by combining n first-order models and considering Eq. (8) and Eq. (11) such as Fig. 8 shows.

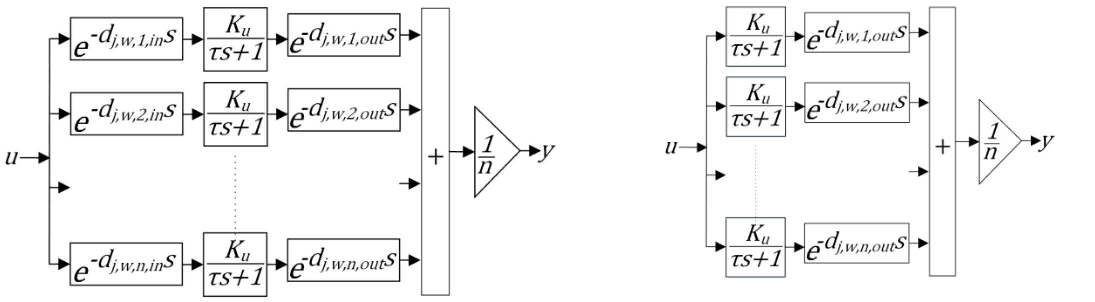

a) Schematic diagram when the input *u* is the inlet temperature

b) Schematic diagram when the input *u* is the water flow rate, the irradiance or the ambient temperature.

Fig. 8: Outlet temperature model combining first-order models.

Notice that the inlet delay is only considered when the input of the first-order models is the inlet temperature. Irradiance, ambient temperature and water flow rate changes affect to the absorber pipes at the same time, the only delay in these cases is the transport delay of the water to go across the outlet connection pipe. Nevertheless, the ambient temperature is assumed constant and its effect is not evaluated with the first-order model because the variation of this input is negligible inside a temporal window equivalent to the observed delay.

Once the models have been implemented, the results have been compared to real data. Since the goal is to evaluate the apparent delay obtained using first-order models, the other inputs must be maintained as constant as possible. Therefore, to compare the experimental and real delay related with the flow rate, irradiance and inlet temperature must be maintained constant.

Fig. 9 represents the recording data of December 21st, 2016. The test consists in applying a step signal (from 35 L·min^{-1} to 30 L·min^{-1}) at the inlet flow of the loop 5, Q_5. The linearized model is obtained around an operational point set up by the outlet temperature around 73 °C, the irradiance level is about 860 W·m^{-2} and the inlet temperature was maintained constant in 55 °C. Notice that the variation of the ambient temperature in that time interval is less than 0.5 °C and the contribution of this input in the linearized model is neglected.

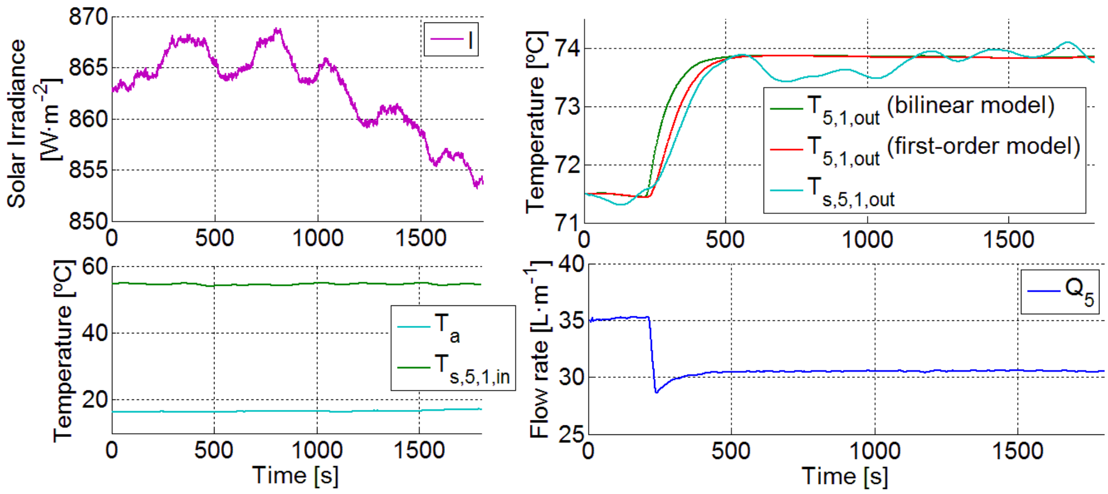

Fig. 9: Experimental disturbances, outlet temperature and simulation results when a flow rate step input is applied, loop 5, section 1, December 21st 2016.

Fig. 9 shows that the lumped parameter model gives a result without including any type of delay. On the other hand, the set of n first order models obtained delivers the total temperature of the loop with an apparent delay when there are changes in the inlet flow rate, which is the hypothesis set out at the beginning. As can be observed the obtained delay is quite similar to the real one.

As commented previously, changes of the solar radiation over the solar field also generate an apparent delay at the outlet temperature (see Fig. 10).

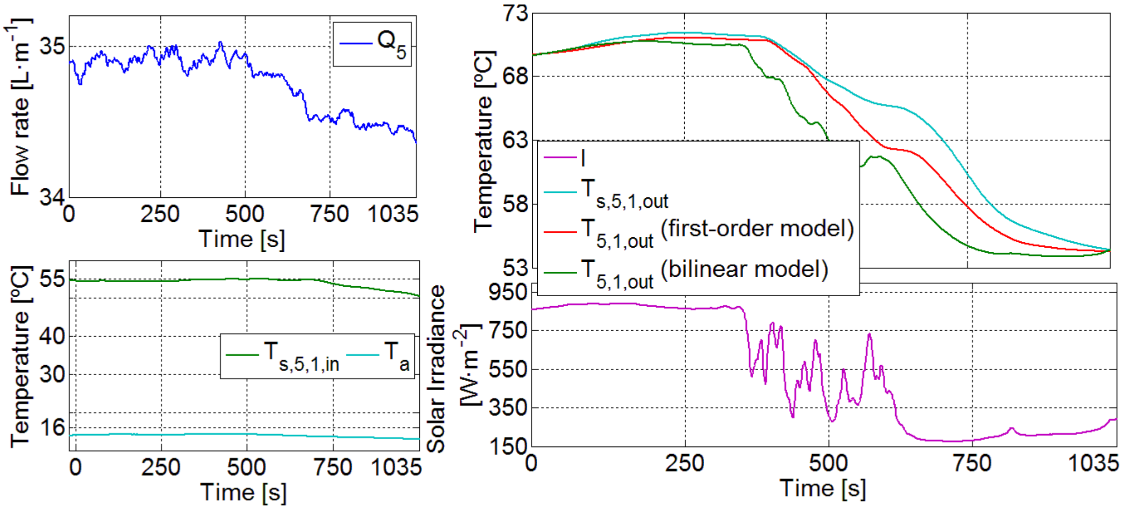

Fig. 10: Experimental disturbances and simulation results using solar irradiance step input, loop 5, section 1, December 14th2016.

4.3 The bilinear model with delays

From the results obtained in the above section, it is demonstrated the existence of the transport delay that can be treated as different input apparent delays. With the aim of improving the results of the bilinear model, it is necessary to introduce these delays in the inputs, as it shown in Eq. (17) and (18).

$$\rho c_p A_{cs} \frac{\partial T_{j,w,out}(t)}{\partial t} = \beta I\left(t - d_{j,tout-I}\right) - \frac{H}{L}\left(T_m(t) - T_a(t)\right) - c_p \frac{\rho}{c_f} Q_j\left(t - d_{j,tout-Q}\right) \frac{\left(T_{j,w,out}(t) - T_{j,w,in}\left(t - d_{j,tout-tin}\right)\right)}{L}, \tag{17}$$

$$T_m(t) = \frac{T_{j,w,out}(t) + T_{j,w,in}(t - d_{j,tout-tin})}{2}. \tag{18}$$

Experiments in the real plant and in the linearized model (see Fig. 11) show that the relationship between flow rate and the delay can be approximated as quadratic functions. For the solar irradiance only simulations with the linearized models have been used.

Eq. (19) to (24) give the approach obtained for the inlet- outlet time delay ($d_{j,tout-tin}$), flow rate-outlet time delay ($d_{j,tout-Q}$) and solar irradiance time delay ($d_{j,tout-I}$).:

$$d_{j,tout-tin} = 0.24 \cdot {Q_j}^2 - 18.42 \cdot Q_j + 480.7, \tag{19}$$

$$d_{j,tout-Q} = 0.13 \cdot {Q_j}^2 - 9.9 \cdot Q_j + 210.17, \tag{20}$$

$$d_{j,tout-I} = 0.124 \cdot {Q_j}^2 - 9.43 \cdot Q_j + 201.38, \tag{21}$$

$$d_{1,tout-tin} = 2.6 \cdot {Q_1}^2 - 86.3 \cdot Q_1 + 876.2, \tag{22}$$

$$d_{1,tout-Q} = 0.11 \cdot {Q_1}^2 - 3.87 \cdot Q_1 + 64, \tag{23}$$

$$d_{1,tout-I} = 0.067 \cdot {Q_1}^2 - 3.12 \cdot Q_1 + 61.1, \tag{24}$$

where j is the loop number ($j \in [2,5]$) and loop 1 is depicted by its own equation due to the difference in the number of absorber tubes.

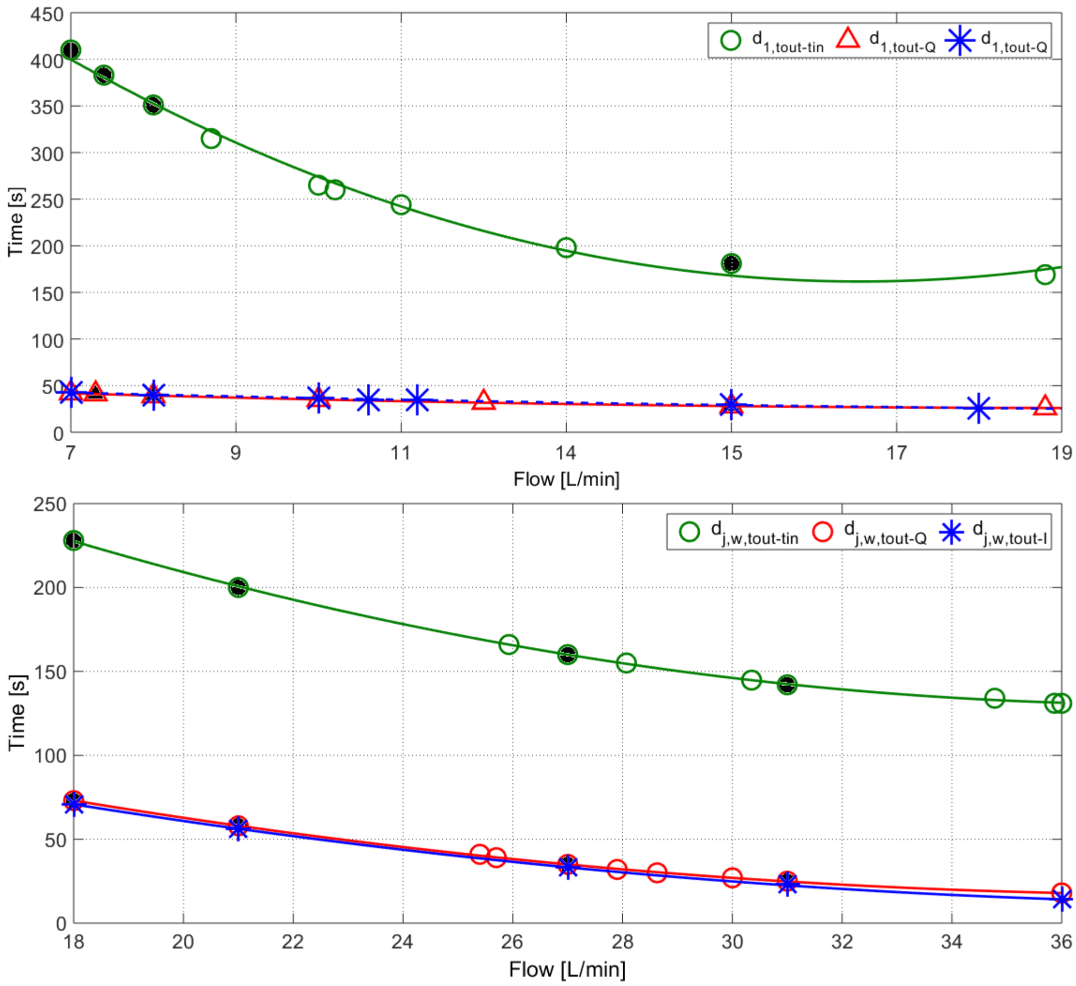

Fig. 11: Outlet temperature time delay curve. Black markers are the experimental data.

Although these equations have been obtained from steady state conditions, the delays are also a good approach for transient data as will be shown in the following results.

If the delays in the form of quadratic functions are included in the bilinear model, the EM and RMSE errors are considerably reduced. As an example, Fig. 12 compares the real data with the results obtained with the bilinear model with and without delays aiming to demonstrate the improvements in the transient performance.

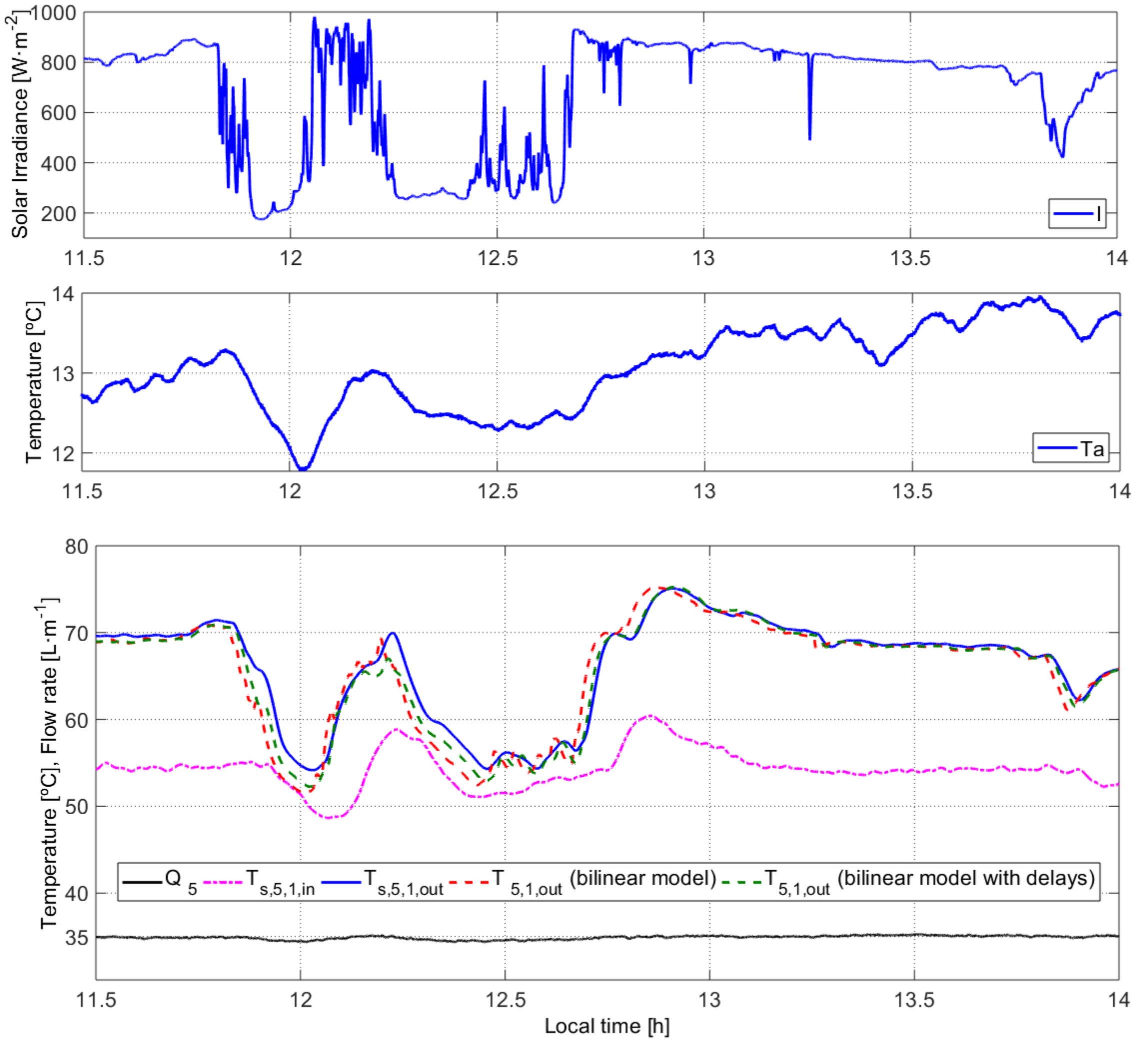

Fig. 12: Experimental disturbances and simulation results using the solar field model including delays, loop 5, section 1, December 14th, 2016

For the case of loop 5 shown in Fig. 12, the water flow rate was maintained constant to 35 $L{\cdot}min^{-1}$. The inlet temperature was controlled with the air-cooler to 55 ºC, but due to irradiance disturbances, it varies between 49 ºC and 61 ºC. This figure shows that under hard solar radiation disturbances, the model with delays improves the results obtained in the previous section.

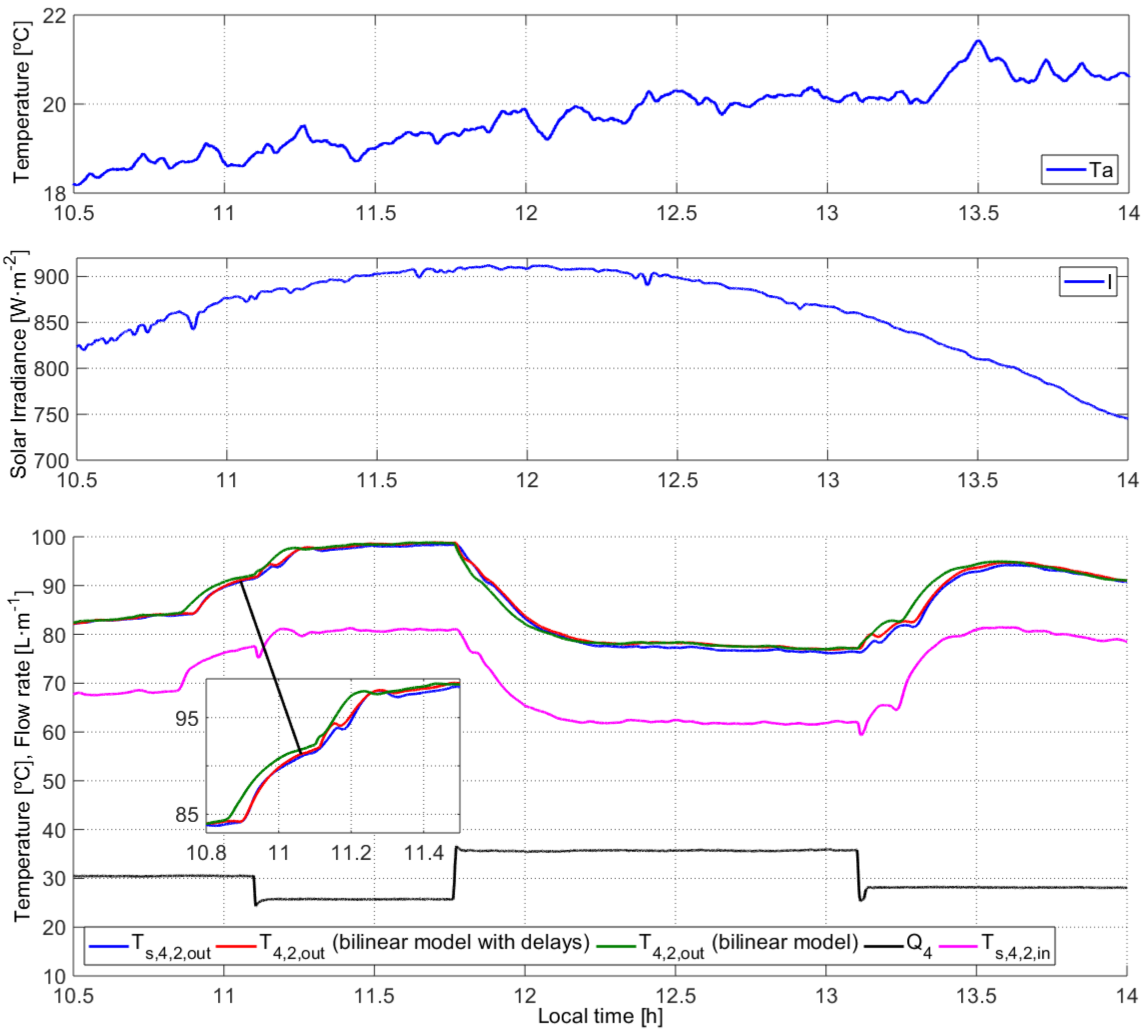

Fig. 13: Experimental disturbances and simulation results using the solar field model, loop 4, section 2, November 17th, 2016

Another example is shown in Fig. 13 for the case of water flow rate and inlet temperature steps performed on November 17th, 2016. The characteristics of this day are the following ones:

- In the test day, solar irradiance does not show cloudy conditions or transitions.
- Ambient temperature varies between 18 ºC and 21 ºC.
- Inlet temperature for Loop 4 varies between 45 ºC and 60 ºC in section 1 and between 62 ºC and 83 ºC in section 2. The inlet flow rate varies between 25 L·min^{-1} and 36 L·min^{-1}.
- The results obtained with the model including delays are quite similar to the real data, being the biggest difference 3.1 ºC at 13:15am (13.25) and 13:50pm (13.5) that occurs by a hard disturbance in the inlet temperature.

The RMSE and ME errors obtained using the bilinear model with delays are included in Table 3. The results demonstrate a notorious reduction of the EM and RMSE errors in comparison with the errors described in Table 2.

Table 3: Campaign results using the bilinear model with delays.

LOOP-SECTION	*PARAMETERS*		*GLOBAL ERROR*	
	H [*J s*$^{-1}$ *°C*$^{-1}$]	*β* [*m*]	*RMSE* [*°C*]	*ME* [*°C*]
5-1	*1.095*	*0.0959*	*2.170*	*4.610*
5-2	*1.106*	*0.0956*	*0.830*	*3.240*
4-1	*1.137*	*0.0949*	*0.860*	*2.640*
4-2	*1.159*	*0.097*	*0.833*	*3.820*
3-1	*1.101*	*0.0951*	*0.930*	*3.340*
3-2	*1.121*	*0.0946*	*0.960*	*4.280*
1	*1.107*	*0.094*	*0.990*	*3.670*

5. A simplified model for control purposes.

As indicated in the preceding section, the solar field model study has been divided into two parts aimed to demonstrate the validity of solar field model; the bilinear model and the input delays. Parametric equations to evaluate the delay for each input have been identified to reduce the error of the model obtained mainly during transients. Nevertheless, in order to obtain the water temperature at the outlet of each loop, two bilinear models are required for each loop. With the aim of reducing the computational time and making the model of each loop easier to be used for control purposes, a simplified model is proposed in this section. The idea is to use just one bilinear equation to evaluate the outlet temperature for each loop and include parametric equations to take into account the delays at the input:

$$\rho c_p A_{cs}\frac{\partial T_{j,out}(t)}{\partial t} = \beta I\left(t-d_{j,tout-I,s}\right) - \frac{H}{L}\left(\frac{T_{j,out}(t)+T_{j,in}(t-d_{j,tout-tin,s})}{2} - T_a(t)\right) - c_p\frac{\rho}{c_f}Q_j\left(t-d_{j,tout-Q,s}\right)\frac{\left(T_{j,out}(t)-T_{j,in}\left(t-d_{j,tout-tin,s}\right)\right)}{L}, \quad (25)$$

where j is the loop number ($j \in [1,5]$) and the delays for the simplified model are the following ones:

$$d_{j,tout-Q,s} = 2\cdot d_{j,tout-Q} + 0.037\cdot {Q_j}^2 - 3.37\cdot Q_j + 92.63 \quad (26)$$

$$d_{j,tout-tin,s} = 2\cdot d_{j,tout-tin} + 0.037\cdot {Q_j}^2 - 3.37\cdot Q_j + 92.63 \quad (27)$$

$$d_{j,tout-I,s} = 2\cdot d_{j,tout-I} + 0.037\cdot {Q_j}^2 - 3.37\cdot Q_j + 92.63 \quad (28)$$

These equations include the delays obtained in Eq. (19) to (21), but multiplied by 2, because the simplified model incorporates the two sections of each loop in only one model, this means, that number l of absorber pipes pipe ($l \in [1{,}700]$) and the total distance from the beginning of the loop ($T_{s,j-k,in}$ [°C]) to the last absorber ($l = 700$) has been increased. Furthermore, the transport delay in the pipe between the end of section 1 and the beginning of section 2 has been added to Eq. (26) to (28). This transport delay has been estimated using Eq. (5) as described by (Normey-Rico *et al.*, 1998) as well as in section 4.

Once the delays are included, parameters H and β have been calibrated again (see Table 4) with data from the experimental campaign carried on for the calibration process.

Fig. 14 shows the model validation with data from the test carried on in November 16th, 2016 in which several changes were performed in the inlet flow rate. As can be seen, the results of the simplified model including the delays are very similar to real data. The characteristics of this day are the following ones:

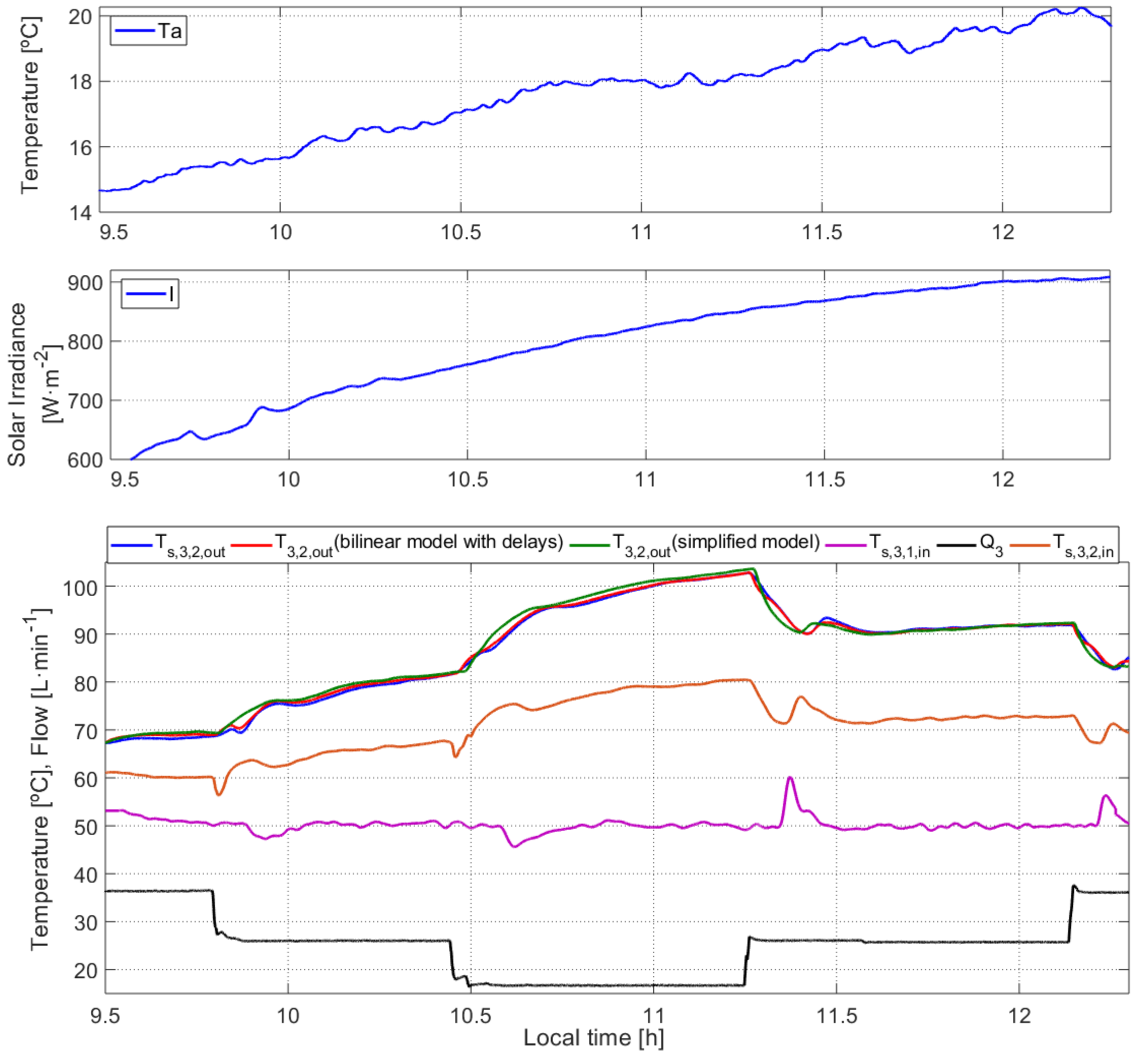

Fig. 14: Experimental disturbances and simulation results using the solar field model, loop 3, section 2, November 16th, 2016

- In the test day, solar irradiance does not show cloudy conditions or transitions.
- Ambient temperature varies between 14 ºC and 20 ºC.
- Inlet temperature for the loop 3 remains almost constant at 50 ºC. The inlet flow rate varies between 18 L·min^{-1} and 36 L·min^{-1}.
- The comparison between the simulated and the real loop outlet temperature shows that the biggest difference is 3.53 ºC at 09:52am (9.88) and 3.1 ºC at 11:16am (11.28).

Notice that using the simplified model the main source of error comes from the fact that the inlet temperature of section two is not considered as model input. Although the outlet temperature of section 1 should be the same than the inlet temperature of section 2 $(T_{j,l,out} \approx T_{j,2,in})$, in some occasions a non-desirable behavior at the inlet temperature of section 2 has been detected; when flow rate steps are performed, inlet temperature in section 2 decreases immediately such as shown in Fig.14. This dynamic, which is not included in the model, is the cause of the error obtained.In order to check the simplified model behavior against solar irradiance disturbances, several tests under cloudy conditions were carried out. The one performed in December 20th, 2016 is shown in Fig. 15. The characteristics of this day are the following ones:

- In the test day, solar irradiance shows cloudy conditions or transitions. The lowest value is 400 W·m^{-2} at 13:00am. As shown in Fig. 15, the most significant disturbances occurred approximately between 11:48am and 13:15pm.

- Ambient temperature varies between 12 ºC and 16 ºC. Inlet flow rate and inlet temperature remain constant.

- The comparison between the simulated and the real solar field outlet temperature can be observed in Fig. 15, where the similarity of the simplified model results with the real ones are noticed, being the biggest difference 3.59 ºC at 12:00pm.

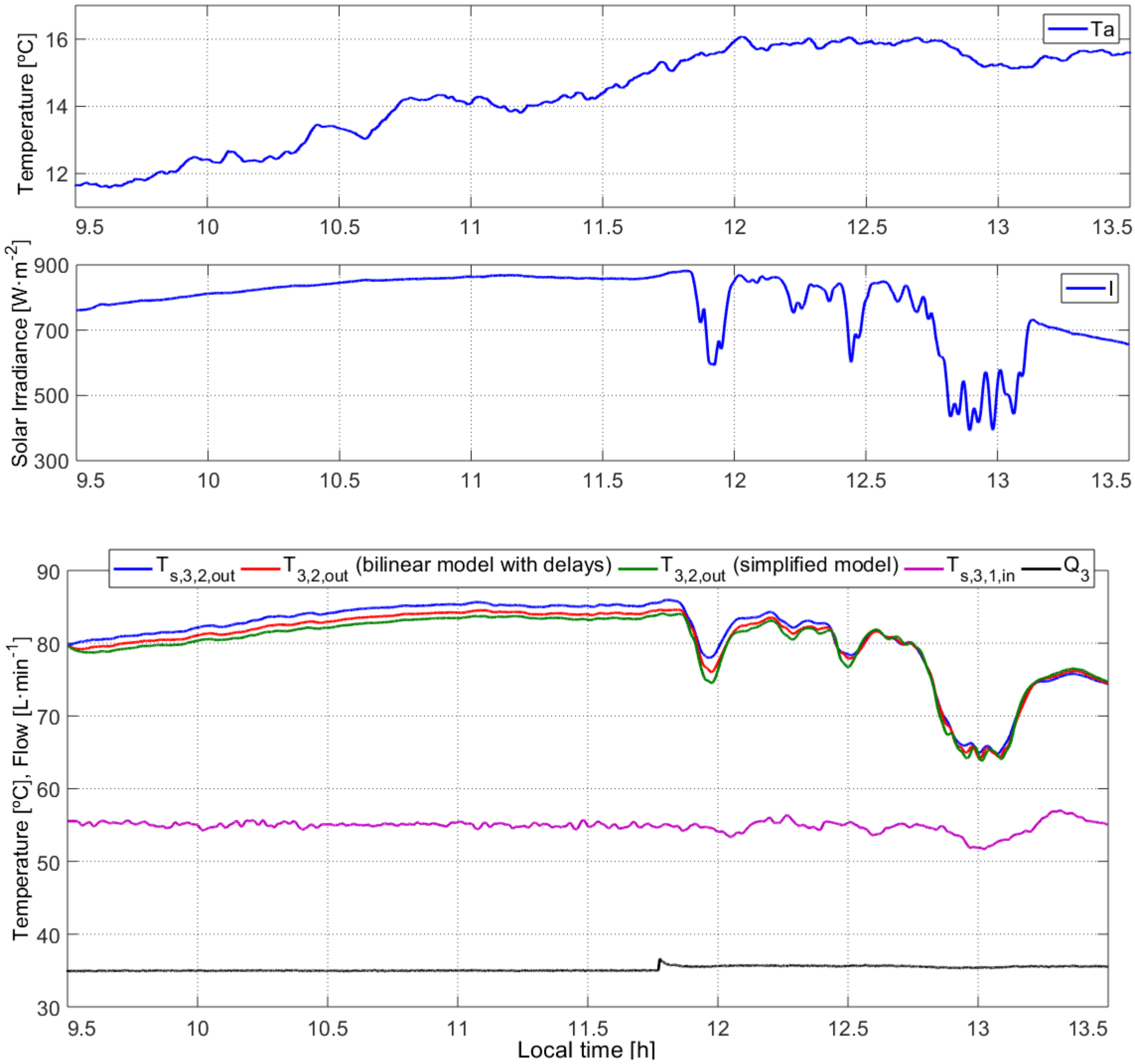

Fig. 15: Experimental disturbances and simulation results using the simplified solar field model, loop 3, section 2, December 20th, 2016

As shown in Table 4, a comparison between the results of the simplified model with the real data outlet temperature is performed. For solar irradiance disturbance the simplified model reacts according to the outlet temperature dynamics but for the inlet flow rate changes the behavior can be a little bit different to the real data, as a result to the non-considered dynamic observed in some occasions in the second section inlet temperature. This makes that the results of the simplified model not as good as expected.

Despite this, the ME and RMSE errors are low and it is possible to infer that the simplified model can be used for future investigations of solar field controllers and MED operating strategies optimization.

Table. 4: Test campaign results with the simplified model.

Loop	*Parameters*		*Global error*	
	H [$J\ s^{-1}\ {}^{o}C^{-1}$]	*β* [*m*]	*RMSE* [°*C*]	*ME* [°*C*]
5	*1.145*	*0.0972*	*2.120*	*4.560*
4	*1.137*	*0.0948*	*1.660*	*4.030*
3	*1.107*	*0.0926*	*1.720*	*4.610*
1	*1.107*	*0.0936*	*1.790*	*5.910*

The simplified model allows estimating the water temperature at the outlet of each loop while reducing the computational time about 16 % (computational time is reduced from 38 to 32 s when a simulation of 10000 s is performed), because it resolves one differential equation per loop while the complete model includes two differential equations per loop. Nevertheless, the simplified model shows more error than the one expected due to a non-desirable behavior that occurs in some experiments at the inlet temperature of the second section when step flow rates are performed. This fact is the cause of an error increment of about 2 ºC in comparison to the complete model. On the order hand, the results of the simplified model with the delays included are quite satisfactory to be used for control purposes.

Conclusions

The simplified model proposed in this paper implements a concentrated parameter model of flat plate collectors augmented with quadratic functions relating flow rate and delay, providing the evolution of outlet temperature. This model shows the following advantages: (i) its implementation is straightforward; (ii) fast computational time simulation; (iii) adequate performance under different conditions of solar irradiance (sunny and cloudy days), and (iv) it describes variable delays from flow, input temperature and irradiance changes. Simulation results compared with real data have shown that modelling errors when changing values of flow rate, inlet loop temperature and solar irradiance are quite low, thus demonstrating that the simplified model is reliable. Real experiments on a solar field have been included to show the obtained promising results.

As demonstrated in (Ampuño et al.,2018), a good approximation to model the outlet temperature of the solar field is considering input-output related transport delays experimentally obtained. Nevertheless, that solution requires an experimental campaign in which all the inputs must be manipulated to cover the operating range, which is impossible for the irradiance variable, as it is not manipulable (it constitutes a disturbance from the control point of view). For small solar fields, a mean value for the irradiance-output transport delay can be assumed, but for large solar fields it is mandatory to define an irradiance-output transport delay as a function of the flow rate. One of the main objectives of the work is to demonstrate the existence of an apparent delay at the output of the flat plate collector solar field due to the parallel connection of the absorber tubes. The raised hypothesis has been demonstrated using linearized process models arranged in parallel, following the layout of the real solar field. In addition, the methodology explained in this paper permits to obtain the apparent delays from the model described in Eq. (1) without additional experimental campaigns

Finally, it is important to mention that obtaining a solar field outlet temperature model is the first step in the goal of designing control systems that: (i) act against disturbances of solar irradiance, (ii) prevent damages in collectors due to high temperatures, (iii) improve the performance when working at low temperatures, (iv) minimize energy consumption of the plant and (v) maximize thermal performance.

Acknowledgements

This work has been funded by the National Plan Projects DPI2014-56364-C2-1/2-R and DPI2017-85007-R of the Spanish Ministry of Economy, Industry and Competitiveness and ERDF funds. Julio E. Normey-Rico thanks CNPq under project 305785/2015-0 for financial support.

References

Ackermann, T., Carlini, E., Bernhard, E., Groome, F., Orths, A., O'Sullivan, J., de la Torre, M. and Silva, V. (2015) 'Integrating Variable Renewables in Europe', *IEEE Power and Energy Magazine*, 13(6), pp. 67–77. doi: 10.1109/MPE.2015.2461333.

Alarcón, D., Blanco, J., Malato, S., Maldonado, M. I. and Fernandez, P. (2005) 'Design and setup of a hybrid solar seawater desalination system : The AQUASOL project', in *ISES 2005 Solar World Congress*. Orlando, FL, USA.

Alarcón, D., García, L. and Blanco, J. (2007) 'Assessment of an absorption heat pump coupled to a multi-effect distillation unit within AQUASOL project', *Desalination*, 212, pp. 303–310. doi: 10.1016/j.desal.2006.10.015.

Alarcón, D., García, L. and Blanco, J. (2010) 'Design recommendations for a multi-effect distillation plant connected to a double-effect absorption heat pump: A solar desalination case study', *Desalination*, 262(1–3), pp. 11–14. doi: 10.1016/j.desal.2010.04.064.

Aleksiejuk, J., Chochowski, A. and Reshetiuk, V. (2018) 'Analog model of dynamics of flat-plate solar collector', *Solar Energy*, 160, pp. 103-116. doi: 10.1016/j.solener.2017.11.079.

Ali, A., Al-karaghouli and Kazmerski, L. L. (2011) *Renewable Energy Opportunities in Water Desalination*. *Desalination, trens and technologies.* InTech. India.

Ampuño, G., Roca, L., Berenguel, M., Gil, J. D., Pérez, M. and Normey-Rico, J. E. (2018) 'Modeling and simulation of a solar field based on flat-plate collectors', *Solar Energy*, 170, pp. 369-378. doi:10.1016/j.solener.2018.05.076.

Ayala, C. O., Roca, L., Guzmán, J. L., Normey-Rico, J. E., Berenguel, M. and Yebra, L. (2011) 'Local model predictive controller in a solar desalination plant collector field.', *Renewable Energy*, 36, pp. 3001–3012. doi: 10.1016/j.renene.2011.03.037.

Brus, L. and Zambrano, D. (2010) 'Black-box identification of solar collector dynamics with variant time delay', *Control Engineering Practice*, 18(10), pp. 1133–1146. doi: 10.1016/j.conengprac.2010.06.006.

Buzás, J. and Kicsiny, R. (2014) 'Transfer functions of solar collectors for dynamical analysis and control design', *Renewable Energy*, 68, pp. 146–155. doi: 10.1016/j.renene.2014.01.037.

Camacho, E. F., Berenguel, M., Rubio, F. R. and Martínez, D. (2012) *Control of solar energy systems*. Springer Science & Business Media. London.

Camacho, E. F., Rubio, F. R. and Berenguel, M. (1997) *Advanced control of solar plants.* Springer. London.

Deng, J., Yang, X. and Wang, P. (2015) 'Study on the second-order transfer function models for dynamictests of flat-plate solar collectors Part I: A proposed new model and a fitting methodology', *Solar Energy*, 114, pp. 418–426. doi: 10.1016/j.solener.2015.01.046.

Deng, J., Yang, X. and Wang, P. (2017) 'Study on the second-order transfer function models for dynamic tests of flat-plate solar collectors Part II: Experimental validation', *Solar Energy*, 141, pp. 334–346. doi: 10.1016/j.solener.2015.01.046.

Duffie, J. A. and Beckman, W. A. (2013) *Solar Engineering of Thermal Processes*. Fourth Ed. New Jersey: John Wiley & Sons, Inc., Hoboken.

Facão, J. (2016) 'Optimization of flow distribution in flat plate solar thermal collectors with riser and header arrangements', *Solar Energy*, 120, pp. 104–112. doi: 10.1016/j.solener.2015.07.034.

Fernández, P., García, L., Alarcón, D., Palenzuela, P. and Martín, I. (2012) 'Experimental analysis of a multi-effect distillation unit operated out of nominal conditions', *Desalination*, 284, pp. 233–237. doi: 10.1016/j.desal.2011.09.004.

Fischer, S., Heidemann, W., Müller-Steinhagen, H., Perers, B., Bergquist, P. and Hellström, B. (2004) 'Collector test method under quasi-dynamic conditions according to the European Standard EN 12975-2', *Solar Energy*, 76(1–3), pp. 117–123. doi: 10.1016/j.solener.2003.07.021.

Gil, J. D., Roca, L., Zaragoza, G. and Berenguel, M. (2018) 'A feedback control system with reference governor for a solar membrane distillation pilot facility', *Renewable Energy*, 120, pp. 536–549. doi: 10.1016/j.renene.2017.12.107.

Goodwin, G. C. and Payne, R. L. (1977) *Dynamic system identification. Experiment design and data analysis, Mathematics in Science and Engineering, 136. Academic Press.* London.

Kalogirou, S. A. (2004) 'Solar thermal collectors and applications', *Progress in Energy and Combustion Science*, 30, pp. 231–295. doi: 10.1016/j.pecs.2004.02.001.

Kicsiny, R (2017) ‘Transfer functions of solar heating systems with pipes for dynamic analysis and control design’, *Solar Energy*, 150, pp. 596–607. doi: 10.1016/solener.2017.05.006.

Nayak, J. K. and Amer, E. H. (2000) ‘Experimental and theoretical evaluation of dynamic test procedures for solar flat-plate collectors’, *Solar Energy*, 69(5), pp. 377–401. doi: 10.1016/S0038-092X(00)00108-0.

Normey-Rico, J. E., Bordons, C., Berenguel, M. and Camacho, E. F. (1998) ‘A robust adaptive dead-time compensator with application to a solar collector field’, *IFAC Proceedings Volumes*, 31(19), pp. 93-98. doi: 10.1016/S1474-6670(17)41134-7.

Normey-Rico, J. E. and Camacho, E. F. (2007) *Control of Dead-time Processes*. Springer. London.

Ogata, K. (1998) ‘*Ingeniería de Control Moderna*. Prentice Hall. México.

Pasamontes, M., Álvarez, J. D., Guzmán, J. L. and Berenguel, M. (2009) ‘Hybrid modeling of a solar cooling system’, *IFAC Proceedings Volumes*, 42(17), pp. 26–31. doi: http://dx.doi.org/10.3182/20090916-3-ES-3003.00006.

Pasamontes, M., Álvarez, J. D., Guzmán, J. L., Berenguel, M. and Camacho, E. F. (2013) ‘Hybrid modeling of a solar-thermal heating facility’, *Solar Energy*, 97, pp. 577–590. doi: 10.1016/j.solener.2013.09.024.

Roca, L., Berenguel, M., Yebra, L. and Alarcón-Padilla, D. (2008) ‘Solar field control for desalination plants’, *Solar Energy*, 82(9), pp. 772-786. doi: 10.1016/j.solener.2008.03.002.

Roca, L., Guzmán, J. L., Normey-Rico, J. E., Berenguel, M. and Yebra, L. (2009) ‘Robust constrained predictive feedback linearization controller in a solar desalination plant collector field’, *Control Engineering Practice*. 17(9), pp. 1076–1088. doi: 10.1016/j.conengprac.2009.04.008.

Romera Cabrerizo, J.A., Santos, M., (2017) ‘ParaTrough: Modelica-based simulation library for solar thermal plants’, *Revista Iberoamericana de Automática e Informática Industrial*, 14(4), 412-423. doi: 10.1016/j.riai.2017.06.005.

Tagliafico, L. A., Scarpa, F. and De Rosa, M. (2014) ‘Dynamic thermal models and CFD analysis for flat-plate thermal solar collectors - A review’, *Renewable and Sustainable Energy Reviews*, 30, pp. 526–537. doi: 10.1016/j.rser.2013.10.023.

Torrico, B. C., Roca, L., Normey-Rico, J. E., Guzmán, J. L. and Yebra, L. (2010) ‘Robust nonlinear predictive control applied to a solar collector field in a solar desalination plant’, *IEEE Transactions on Control Systems Technology*, 18(6), pp. 1430–1439. doi: Doi 10.1109/Tcst.2009.2039137.

Torrico, B. C., Roca, L., Normey-Rico, J. E., Guzmán, J. L. and Yebra, L. (2009) ‘Predictive temperature control of solar collectors in a desalination plant’, in *Proc. European Control Conf.* 23–26, Budapest, Hungary, pp. 4199–4204.